ISSN 1808-8546 (ONLINE) 1808-3765 (CD-ROM)

ESTIMATIVA DA EVAPOTRANSPIRAÇÃO REAL E MAPEAMENTO DE ÁREAS CULTIVADAS EM UMA BACIA DO PROJETO DE INTEGRAÇÃO DO SÃO FRANCISCO (PISF), SEMIÁRIDO PERNAMBUCANO

LIZANDRA DE BARROS DE SOUSA[1]; ABELARDO ANTÔNIO DE ASSUNÇÃO MONTENEGRO[1]; THIERES GEORGE FREIRE DA SILVA[2]; AILTON ALVES DE CARVALHO[1] E MOISÉS ALVES DA SILVA NETO[3]

[1] Departamento de Engenharia Agrícola (DEAGRI). Programa de Pós-Graduação em Engenharia Agrícola (PGEA). Universidade Federal Rural de Pernambuco (UFRPE). Rua Dom Manuel de Medeiros, S/N, Dois Irmãos, CEP: 52171-900, Recife/PE, Brasil. E-mail: lizandradebarros@gmail.com; montenegro.ufrpe@gmail.com; Ailtonalvesst@gmail.com.
[2] Unidade Acadêmica de Serra Talhada (UAST). Universidade Federal Rural de Pernambuco (UFRPE). Avenida Gregório Ferraz Nogueira, S/N, José Tomé de Souza Ramos, CEP: 56909-535, Serra Talhada/PE, Brasil. E-mail: thigeoprofissional@hotmail.com.
[3] Departamento de Engenharia Agrícola (DEAGRI). Universidade Federal Rural de Pernambuco (UFRPE). Rua Dom Manuel de Medeiros, S/N, Dois Irmãos, CEP: 52171-900, Recife/PE, Brasil. E-mail: moisesneto179@gmail.com.

1 RESUMO

A região semiárida brasileira apresenta limitada disponibilidade de recursos hídricos, além disso, profundas alterações no uso e ocupação do solo estão previstas para ocorrer nas bacias hidrográficas de Pernambuco. Objetivou-se avaliar a evapotranspiração real e mapear áreas cultivadas por meio de sensoriamento remoto, utilizando, respectivamente, os modelos SAFER (*Simple Algorithm for Evapotranspiration Retrieving*) e SUREAL (*Surface Resistance Algorithm*), na Bacia do rio Terra Nova, em trecho perenizado. Imagens do satélite Landsat-8, de 2015 a 2020, foram selecionadas. Calculou-se: Índice de Vegetação da Diferença Normalizada (NDVI), albedo, temperatura de superfície, evapotranspiração de referência e evapotranspiração real. As imagens foram processadas no *Google Earth Engine* (GEE) e no *software* QGIS 3.16. Notou-se aumento no índice de cobertura vegetal. Regiões com maiores valores de evapotranspiração real estão ligadas àquelas com temperaturas mais baixas. Observou-se uma menor quantidade de áreas cultivadas no trecho do Rio Terra Nova nas imagens de 2015. Verificou-se o aumento da agricultura na região às margens desse rio, em seu trecho perenizado, de 29,5; 15,2; 7,7; 7,6; e 12,9 km² em 18/07/2016, 22/06/2018, 28/10/2018, 13/11/2018, e 20/12/2020, respectivamente. Além da intensidade de precipitação, a liberação das águas do PISF pode ter contribuído para o aumento de áreas irrigadas na região.

Palavras-chave: sensoriamento remoto, agricultura irrigada, SAFER, SUREAL.

SOUSA, L. B.; MONTENEGRO, A. A. A.; SILVA, T. G. F.; CARVALHO, A. A.; SILVA NETO, M. A.
ESTIMATION OF ACTUAL EVAPOTRANSPIRATION AND MAPPING OF CULTIVATED AREAS IN A BASIN OF THE SÃO FRANCISCO INTEGRATION PROJECT (PISF), SEMIARID OF PERNAMBUCO STATE

Recebido em 25/01/2021 e aprovado para publicação em 03/11/2021
DOI: http://dx.doi.org/10.15809/irriga.2021v26n3p565-583

2 ABSTRACT

The Brazilian semi-arid region has limited availability of water resources, in addition, profound changes in land use and occupation are expected to occur in the river basins of Pernambuco. The objective was to evaluate the actual evapotranspiration and to map cultivated areas through remote sensing, using, respectively, the SAFER (Simple Algorithm for Evapotranspiration Retrieving) and SUREAL (Surface Resistance Algorithm) models, in the Terra Nova River Basin, in a perennial stretch. Landsat-8 satellite images from 2015 to 2020 were selected. The Normalized Difference Vegetation Index (NDVI), albedo, surface temperature, reference evapotranspiration, and actual evapotranspiration were calculated. Images were processed using the Google Earth Engine (GEE) platform and QGIS 3.16 software. There was an increase in the vegetation cover index. Regions with higher actual evapotranspiration values are linked to those with lower temperatures. It was observed a smaller number of cultivated areas in the Terra Nova River stretch in the 2015 images. Also, it was verified an increase in agriculture in the riverside region along this, in its perennial stretch, of 29.5; 15.2; 7.7; 7.6; and 12.9 km² on 07/18/2016, 06/22/2018, 10/28/2018, 11/13/2018, and 12/20/2020, respectively. In addition to the intensity of precipitation, the release of PISF waters may have contributed to the increase in irrigated areas in the region.

Keywords: remote sensing, irrigated agriculture, SAFER, SUREAL.

3 INTRODUCTION

The semiarid region of Northeast Brazil has limited water resources due to irregular rainfall patterns (rainfall poorly distributed temporally and spatially), high evapotranspiration rates, and shallow soils with low water retention capacity. Therefore, water management in river basins is essential for the sustainable development of this region (MONTENEGRO *et al*., 2013).

In the São Francisco River Basin, several irrigated crop areas can be observed (TEIXEIRA *et al*., 2021). Furthermore, profound changes in land use and occupation are expected to occur in the Pernambuco River Basin, whether due to natural causes related to climate change or induced by the implementation of the São Francisco River Integration Project (PISF) with the river basins in Northeast China.

In this sense, new technologies using satellite images to support rational water management in agriculture have gained prominence in the last two decades. (CANCELA *et al* ., 2019) . To achieve sustainable development at the river basin scale, The use of tools that determine real evapotranspiration (ETr) on a large scale is essential.

A simple algorithm *for evapotranspiration-retrieving* (SAFER) was developed and calibrated for semiarid regions (TEIXEIRA, 2010; TEIXEIRA *et al* ., 2015) and can be applied with high precision to estimate ET via satellite images; this algorithm is widely used in Brazil (SILVA; MANZIONE; ALBUQUERQUE FILHO, 2018; FILGUEIRAS *et al*., 2019; VENANCIO *et al*., 2021). Together with the *surface resistance algorithm* (SUREAL) for the classification of vegetation in irrigated crops and natural vegetation, it is possible to evaluate irrigated areas with high spatial resolution, allowing crop management with precision and speed (TEIXEIRA *et al* ., 2014; TEIXEIRA *et al* ., 2017; TEIXEIRA *et al* ., 2021) .

Google *Earth Engine (GEE) is a high-performance computing service platform that combines a catalog of multiple* *satellite images and* geospatial datasets with planetary-scale analysis capabilities via Google's cloud infrastructure technology. It enables the analysis and monitoring of deforestation, droughts, disasters, disease, food security, water management, climate monitoring, and environmental protection. However, in Brazil, its use is still recent, as among those currently underway, the MapBiomas project (2021) stands out, an annual land use and land cover monitoring initiative that uses GEE in Landsat 5, 7, and 8 images (GORELICK *et al*., 2017; SILVA, 2020; GOOGLE EARTH ENGINE, 2021).

Therefore, the objective of this study was to evaluate actual evapotranspiration and map irrigated crops via remote sensing, applying the SAFER and SUREAL algorithms, respectively, in a GHG environment in the São Francisco Basin, surrounding the Terra Nova River, a semiarid region in Pernambuco, and partially perennialized by the São Francisco River Integration Project. Such analyses are essential for environmental planning and water resource management in regions among different sectors of society.

4 MATERIALS AND METHODS

4.1 Study area

The study was carried out in the São Francisco Basin in its submiddle stretch in the state of Pernambuco. Specifically, an area south of the Terra Nova River Basin was analyzed in the municipality of Cabrobó, which is located at geographic coordinates 08°30'51” S and 39°18'36” W. This area is located in the São Francisco Mesoregion and the Petrolina Microregion of the state of Pernambuco, approximately 536.1 km from the capital, Recife, occupying an area of 1658.62 km², which represents a total of 1.65% of the state (MINERAL RESOURCES RESEARCH COMPANY, 2005; IBGE, 2021; PERNAMBUCAN WATPANER AND CLIMATE AGENCY, 2021). For the analysis of irrigated agriculture on the banks of the Terra Nova Stream, a distance of 5 km was considered for each bank from the riverbed, starting at the point of release of water from the São Francisco River Integration Project to the mouth of the Terra Nova River (Figure 1).

Figure 1. Location map of the stretch of the Terra Nova Stream, which is the subject of the study.

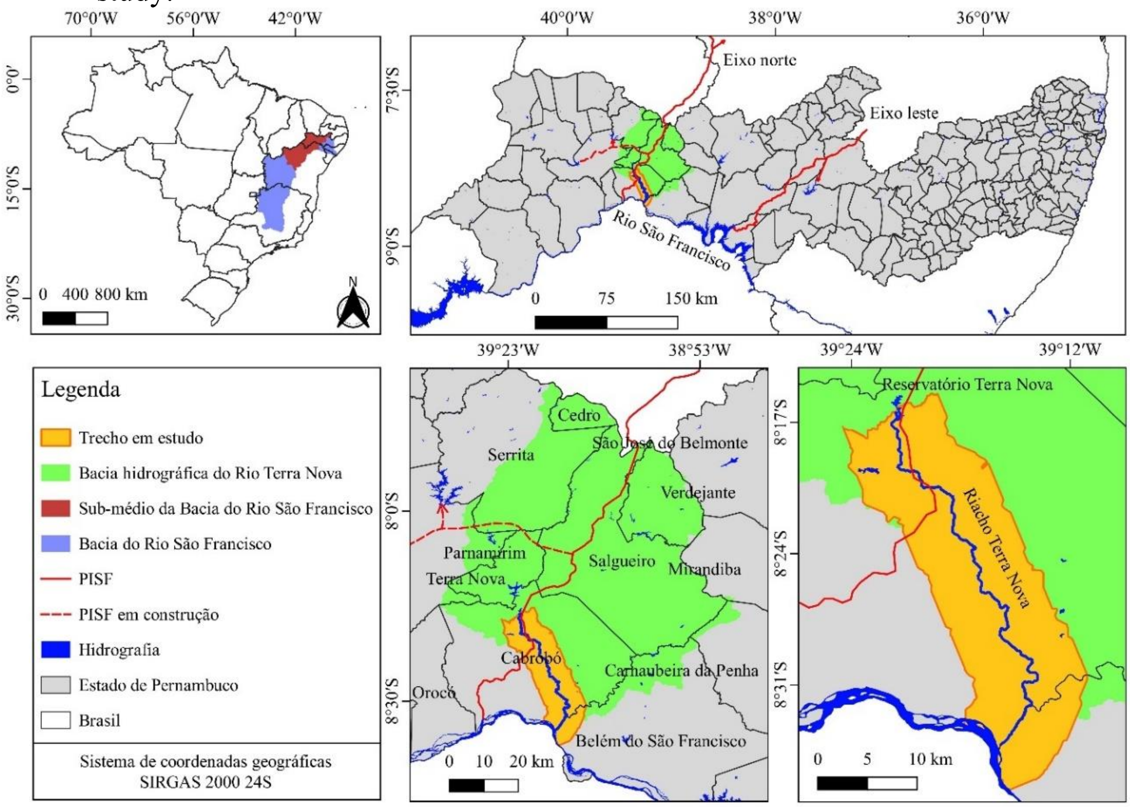

Source: prepared by the authors.

According to the Köppen climate classification, the climate of the basin and the municipality is hot semiarid, BSh (ALVARES *et al*., 2013; BECK *et al*., 2018). The region's average annual rainfall is less than 1,000 mm, and the relief, which varies from flat to undulating, is generally covered by hyperxerophilic Caatinga. Furthermore, vegetation and land use include portions of savanna formation and areas occupied by agricultural/livestock activities. Three soil types predominate in the basin: Neossolos Fluvic, Planosols and Luvisols (INCRA, 2016). For the studied area, the soils are Neosols Litholic and Fluvic, Planossolo Natric and Chromic Luvisol.

4.2 Meteorological data and satellite imagery (Landsat 8 OLI/TIRS)

Meteorological data such as air temperature (T, °C), wind speed at 10 m height (u_{10}, m s^{-1}), solar radiation (Ra, MJ m^{2} d^{-1}), relative humidity (RH, %) and precipitation (mm) were obtained through the National Institute of Meteorology (INMET) from an automated meteorological station located in the municipality of Cabrobó, PE. These data were used to determine the daily reference evapotranspiration (ET) via the Penman–Monteith method of the *Food and Agriculture Organization of the United* Nations (FAO), Equation 1 (ALLEN *et al*., 1998). This method is widely used to determine reference evapotranspiration and manage irrigation at the field level (BEZERRA *et al*., 2010).

$$ET_{0(24h)} = \frac{0{,}408\Delta(R_n - G) + \gamma \frac{900}{T+273} u_2 (e_s - e_a)}{\Delta + \gamma(1 + 0{,}34 u_2)} \quad (1)$$

where R_n is the net radiation (W m $^{-2}$); G (W m $^{-2}$) is the ground heat flux; γ is the psychrometric constant (kPa °C $^{-1}$); T is the mean daily air temperature (°C); u_2 is the mean daily wind speed at a height of 2 m (ms $^{-1}$), whose value was previously adjusted via Equation 2 (ALLEN *et al*., 1998; BEZERRA *et al*., 2010), since the available measurements were collected at a height of 10 m; $_s$ is the saturation pressure (kPa); $_a$ is the actual vapor pressure (kPa); $_s$ - e_a is the vapor pressure deficit (kPa); and Δ is the tangent to the vapor pressure curve (kPa °C $^{-1}$).

$$u_2 = u_{10} \frac{4{,}87}{\ln(67{,}8z - 5{,}42)} \quad (2)$$

where u_{10} is the wind speed measured at a height of 10 m and where z is the height (10 m).

Cloud-free images from the *Operational Land Imager* (OLI) and *thermal sensors were used. Infrared sensor* (TIRS) aboard the Landsat 8 satellite (orbital 216 and point 66). For the OLI sensor, multispectral bands 1 to 7 were used, with a spatial resolution of 30 m, and for the TIRS sensor, thermal bands 10 and 11, with a spatial resolution of 100 m, were resampled to 30 m (UNITED STATES GEOLOGICAL SURVEY, 2016). Climatological data were used in conjunction with twelve images from the Landsat 8 satellite, involving different conditions throughout the years 2015--2020, as shown in Table 1.

Table 1. Image date, identification (ID), Julian day (DJ), orbit and satellite point.

Date	ID	DJ	Orbit	Point
11/21/15	LC08_216066_20151121	325	216	66
12/07/15	LC08_216066_20151207	341	216	66
07/18/16	LC08_216066_20160718	200	216	66
09/20/16	LC08_216066_20160920	264	216	66
06/22/18	LC08_216066_20180622	173	216	66
10/28/18	LC08_216066_20181028	301	216	66
11/13/18	LC08_216066_20181113	317	216	66
09/13/19	LC08_216066_20190913	256	216	66
10/15/19	LC08_216066_20191015	288	216	66
11/16/19	LC08_216066_20191116	320	216	66
12/02/19	LC08_216066_20191202	336	216	66
12/20/20	LC08_216066_20201220	355	216	66

Source: United States Geological Survey (2021).

Landsat data are available in the *Google Earth Engine* in several computed products. In this study, the SAFER application methodology of Teixeira *et al. was used.* (2009), Teixeira *et al* . (2013), and Teixeira *et al. . (2017), three* Landsat 8 imagery products were used: raw (DN), top-of-atmosphere reflectance (TOA), and surface reflectance (SR) products. The raw images were used only in the conversion of the spectral radiances of bands 10 and 11 (thermal bands), according to the methodology of Teixeira *et al*. (2017) and Filgueiras *et al*. (2019), Equation 3.

$$L_\lambda = M_L * DN + A_L \quad (3)$$

where L_λ is the spectral radiance (W m $^{-2}$ sr $^{-1}$ μm $^{-1}$) for the thermal bands (0.00033420); M_L is the multiplicative factor specific to each band; DN is the pixel value (DN) of the standard product (raw image); and A_L is the additive factor specific to each band (0.10000).

To calculate the normalized difference vegetation index (NDVI), the surface reflectance product (with atmospheric correction) was used, which was performed via the *Land Surface Reflectance Code* (LaSRC) developed by *the United States Geological Survey* (USGS) (2020). In the other processing, the reflectance product at the top of the atmosphere was used, with radiometric calibration, in which the calibration coefficients are extracted from the image metadata, with more details of the calculation in Chander, Markham and Helder (2009).

4.2 Simple Algorithm for Evapotranspiration Retrieval (SAFER)

The SAFER model requires remote sensing data, namely, the normalized difference vegetation index (NDVI), planetary albedo (α_{TOA}), surface albedo (α_0), brightness temperature (T_{bright}), and surface temperature (T_0), in addition to the combination of these data with the reference evapotranspiration (ET_0). The SAFER application steps are described according to Teixeira *et al*. (2013) and Teixeira *et al*. (2017), as summarized in Figure 2.

Figure 2. *Simple* processing flowchart *Algorithm for Evapotranspiration Retrieval* (SAFER). Landsat images in their raw form (DN); top-of-atmosphere reflectance (TOA); surface reflectance (SR); normalized difference vegetation index (NDVI); reference evapotranspiration (ET_0); and actual evapotranspiration (ET).

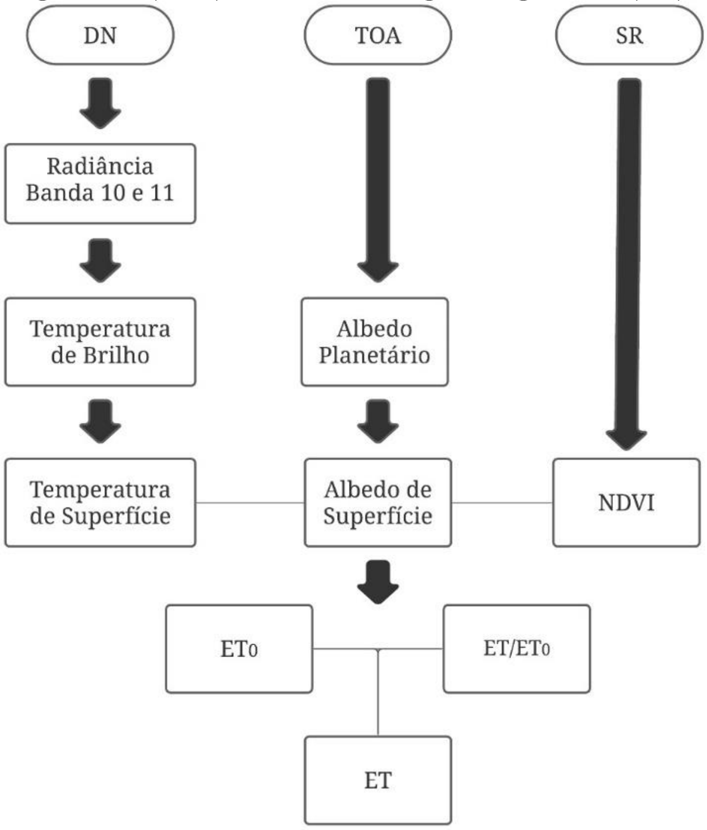

Source: Adapted from Teixeira *et al*. (2013).

To calculate the brightness temperatures of bands 10 and 11 (Landsat 8), the inverse of the Planck equation was applied to the estimated radiation, following the methodology of Teixeira *et al.* (2017), Equation 4.

$$T_b = \frac{K_2}{\ln\left(\frac{K_1}{L_\lambda}+1\right)} \quad (4)$$

where T_b is the satellite brightness temperature (K); L_λ is the spectral radiance (W m^{-2} sr^{-1} μm^{-1}) for the thermal bands (10 and 11); and K_1 and K_2 are the band-specific thermal conversion constants from the metadata. The average value between T_b of band 10 and T_b of band 11 was considered the brightness temperature (T_{bright}).

Subsequently, surface temperatures (with atmospheric correction) were obtained according to the parameterized equation obtained by Teixeira *et al.* (2013), Equation 5.

$$T_0 = 1.07 * T_{bright} - 20.17 \quad (5)$$

where T_0 is the surface temperature (K) and T_{bright} is the brightness temperature (K). The surface temperature was then converted from degrees Kelvin to degrees Celsius to be applied via Equation (9).

The planetary albedo at the top of the atmosphere (α_{TOA}) was calculated as the total sum of the different values of ρ_λ according to the weights for each band (bands 1 to 7), Equation 6 (TEIXEIRA *et al.*, 2017).

$$\alpha_{TOA} = \Sigma(\omega_\lambda * \rho_\lambda) \quad (6)$$

where α_{TOA} is the planetary albedo at the top of the atmosphere; ω_λ is the ratio of the amount of shortwave radiation received from the sun at the top of the atmosphere in a given interval to the sum of all bands used for α_{TOA}; and ρ_λ is the reflectance of the top of the atmosphere for each band.

Then, α_{TOA} was transformed into surface albedo data (with atmospheric correction) by applying Equation 7 obtained by Teixeira *et al.* (2013).

$$\alpha_0 = 0.61 * \alpha_{TOA} - 0.08 \quad (7)$$

where α_0 is the surface albedo and α_{TOA} is the planetary albedo at the top of the atmosphere.

The normalized difference vegetation index (NDVI) was calculated by the ratio of the difference between the near-infrared (ρ_{nir}) and red (ρ_{red}) reflectivities and their sum, according to Equation 8 (ROUSE *et al.*, 1973). Equation 9 does not work for water bodies, so a filter for NDVI > 0 was subsequently applied to remove these pixels from the image.

$$NDVI = \frac{\rho_{nir}-\rho_{red}}{\rho_{nir}+\rho_{red}} \quad (8)$$

After the variables were obtained, the SAFER algorithm was used to model the ratio between the actual evapotranspiration and the reference evapotranspiration ($ET_r / ET_0 = ET_f$) over the area (Equation 9) (TEIXEIRA *et al.*, 2017).

$$ET_f = \exp\left[a + b\left(\frac{T_0}{\alpha_0 * NDVI}\right)\right] \quad (9)$$

where ET_f is the ratio between actual evapotranspiration and reference evapotranspiration; a and b are regression coefficients of 1.8 and -0.008, respectively, which are applicable for the Brazilian semiarid region, according to Teixeira *et al.* (2013); T_0 is the surface temperature (°C); α_0 is the surface albedo; and NDVI is the normalized difference vegetation index.

Actual evapotranspiration (ET_r) was estimated via Equation (10). This calculation is independent of the user's knowledge about land use or the crop used in the field, since the ETf_{ratio} allows inferences about the crop coefficient (FILGUEIRAS *et al.*, 2019).

$$ET_r = ET_0 * ET_f \quad (10)$$

where ET_r is the actual evapotranspiration (mm day $^{-1}$); ET_0 is the reference evapotranspiration according to the FAO Penman–Monteith method (ALLEN *et al.*, 1998) (mm day $^{-1}$); and ET_f is the ratio between the actual evapotranspiration and the reference evapotranspiration.

4.3 Surface resistance algorithm (SUREAL)

According to Teixeira *et al.* (2014), both surface resistance (r_s) and ET_r/ET_0 are related to soil moisture conditions and remote sensing parameters. On this basis, the *surface model resistance algorithm* (SUREAL) was applied for the classification of vegetation into irrigated crops and natural vegetation, Equation 11. Surface resistance values (r_s) below 800 sm $^{-1}$ and an NDVI above or equal to 0.4 are considered irrigated crops, whereas r_s values between 1000 and 10000 sm $^{-1}$ and an NDVI below 0.4 are considered natural vegetation (TEIXEIRA *et al.*, 2017).

$$r_s = \exp\left[a * \left(\frac{T_0}{\alpha_0}\right) * (1 - NDVI) + b\right] \quad (11)$$

where a and b are regression coefficients of 0.04 and 2.72, respectively, for the semiarid conditions of Brazil (TEIXEIRA, 2012; TEIXEIRA *et al.*, 2013; TEIXEIRA *et al.*, 2014). SUREAL was applied to a 1.5 km wide section of each stream bank to filter and separately quantify the agricultural areas on the banks.

4.5 Mapping and descriptive statistics of the data

The results were exported, and the maps were created via QGIS 3.16 *software. The* ET data were subjected to descriptive statistics: minimum, maximum, mean, standard deviation and coefficient of variation.

5 RESULTS AND DISCUSSION

The reference evapotranspiration (ET) from 2015--2020 is illustrated in Figure 3, which uses agrometeorological data from a station located in the municipality of Cabrobó, PE. Precipitation was the most variable climatic parameter, corroborating the findings of Marengo *et al.* (2011), who stated that the semiarid region of Brazil presents rainfall regimes marked by irregular rainfall and poor distribution throughout the years. The minimum ET values generally occurred between January and May. An inverse relationship between precipitation and reference evapotranspiration is noteworthy, which, according to Collischonn and Tucci (2014), is due to greater sunlight and lower humidity on dry days and the higher average air temperature under these conditions.

Figure 3. Daily values of precipitation and reference evapotranspiration (ETo), covering the years 2015--2020, were obtained from the Cabrobó agrometeorological station in the municipality of Cabrobó, PE, Northeast Brazil.

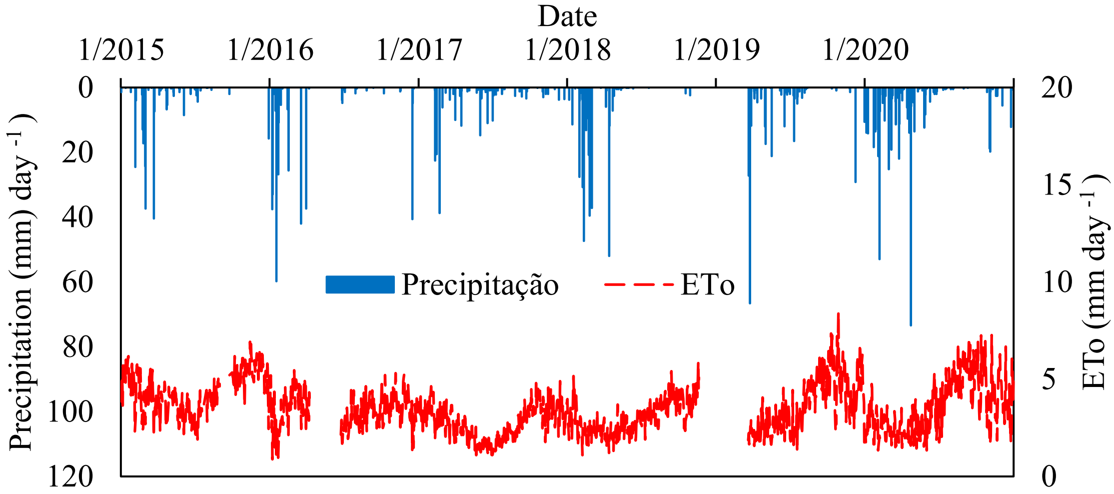

Defining the difference between P and ET_0 as a gross measure of natural water availability (TEIXEIRA *et al*., 2014), from 2015--2020, climatic water surplus ($P > ET_0$) occurred in a few periods, whereas climatic water deficit ($P - ET_0 < 0$) was the most common condition. Therefore, irrigation is essential in this region, especially in the second half of the year (autumn–winter, the driest period).

The precipitation data prior to the imaging dates were analyzed, as shown in Table 2, allowing us to observe the accumulated antecedent precipitation at 30, 60, and 90 days. All accumulated antecedent precipitation over 30 days was low, with maximums of 11 mm occurring on 07/18/2016 and 12/20/2020. After 60 days, the maximum accumulated precipitation (PAM) occurred on 12/20/2020 (57.8 mm), and after 90 days, the PAM occurred on 06/22/2018 (85 mm).

Table 2. Accumulated precipitation (mm) prior to imaging

Dates	Accumulated antecedent precipitation		
	30 days	**60 days**	**90 days**
11/21/15	0	2	2.4
12/07/15	0	0	2.4
07/18/16	11	11	11
09/20/16	1.4	4.4	15.4
06/22/18	1	6.4	85
10/28/18	1.8	1.8	1.8
11/13/18	4.2	4.2	4.2
09/13/19	0	15	59.6
10/15/19	0.4	0.4	15.4
11/16/19	1	1.4	1.4
12/02/19	1.8	3.2	3.2
12/20/20	11	57.8	57.8

With respect to the NDVI of the images (Figure 4), there was an increase in this variable between the images before and after the perennialization of the river (2015). Temporally and spatially, the NDVI variation was high, as shown in Figures 4C, 4E, and 4 L. Therefore, in the 2015 images (Figures 4A and 4B), these areas were less evident on the banks of the Terra Nova Stream. Thus, the release of water from the Terra Nova Reservoir directly influences the increase in vegetation cover and the expansion of crops along banks. Notably, previous precipitation had a significant influence on the results. According to Oliveira *et al*. (2020), the rainfall regime is largely responsible for the availability of biomass in dry areas and is correlated with vegetation cover.

Figure 4. Normalized difference vegetation index (NDVI). 2015-11-21 (A); 2015-12-07 (B); 2016-07-18 (C); 2016-09-20 (D); 2018-06-22 (E); 2018-10-28 (F); 2018-11-13 (G); 2019-09-13 (H); 2019-10-15 (I); 2019-11-16 (J); 2019-12-02 (K); and 2020-12-20 (L).

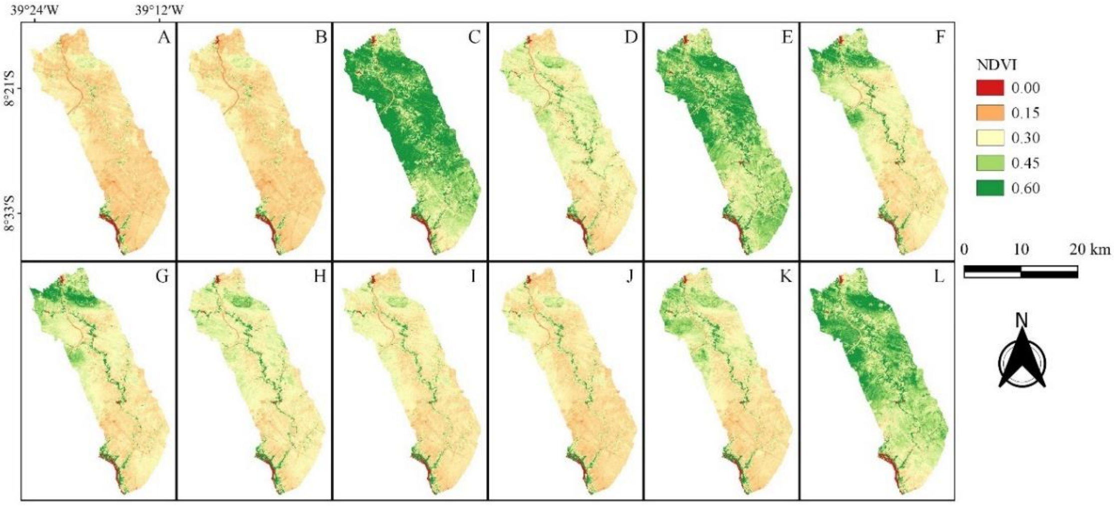

The highest pixel average NDVI values occurred on July 18, 2016 (Figure 4C), followed by June 22, 2018 (Figure 4E) and December 20, 2020 (Figure 4L). Furthermore, from 2016 onward, the banks of the Terra Nova stream experienced a spatial increase in the NDVI (from 0.45 to 0.60) because the rains resulted in high vegetative development in the Caatinga, and agricultural crops developed well because of a regular additional supply of water via irrigation and because of the rains. The lowest average NDVI values occurred in the images from 2015. These results are in agreement with Silva (2020), who noted that NDVI values in the range of 0.15–0.60 may indicate cultivated areas.

The surface albedo (Figure 5) presented low temporal and spatial variability, except on July 18, 2016, June 22, 2018, and December 20, 2020 (Figures 5C, 5E, and 5 L, respectively), and was associated with land use and heterogeneous vegetation cover. The average values ranged from 0.16 to 0.18, with a maximum of 0.31 occurring on November 16, 2019 (Figure 5J), which was the driest period of the studied series. This behavior is in agreement with the low soil moisture, as well as the period of the year that presents high levels of incident global solar radiation (R_g) (SILVA; MANZIONE; ALBUQUERQUE FILHO, 2018). In 2015 and 2016, Lins *et al*. (2017) reported surface albedo values of 0.03--0.20

and greater extensions in areas with vegetation cover, and in less vegetated areas, values of up to 0.45 were found for the municipality of Arcoverde, PE.

Figure 5. Surface albedo. 11/21/2015 (A); 12/07/2015 (B); 07/18/2016 (C); 09/20/2016 (D); 06/22/2018 (E); 10/28/2018 (F); 11/13/2018 (G); 09/13/2019 (H); 10/15/2019 (I); 11/16/2019 (J); 02/12/2019 (K); and 12/20/2020 (L).

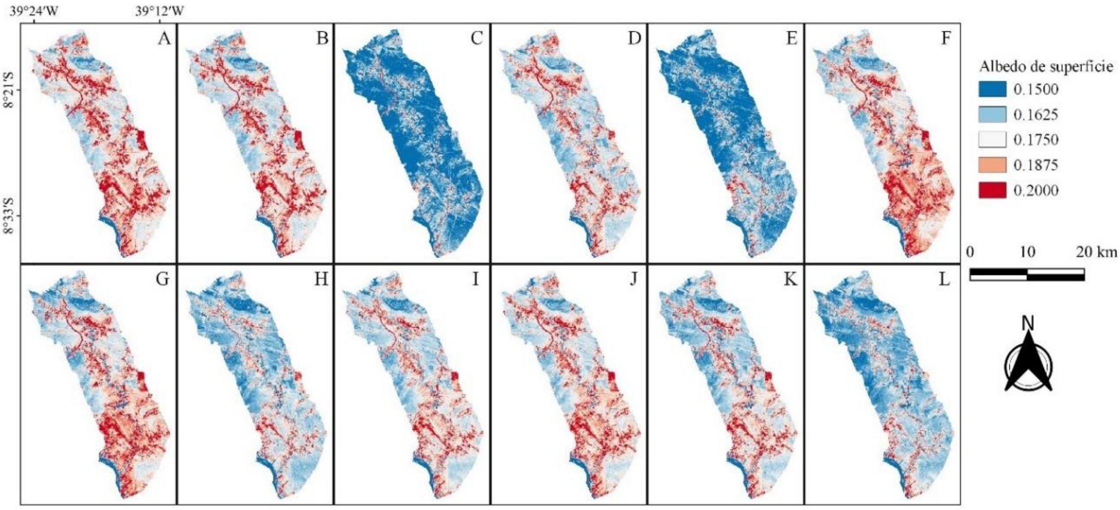

According to Venancio *et al*. (2021), as the surface albedo decreases, an increase in solar energy absorption predominates, increasing the surface temperature and thus contributing to a relative increase in water consumption.

Figure 6 shows the spatial distribution of surface temperature for each image. According to Silva, Manzione, and Albuquerque Filho (2018), surface temperature is related primarily to absorbed solar radiation, which is transformed into thermal energy by the transfer of longwave radiation from surfaces to the atmosphere. The lowest temperatures (blue hues) were found in water bodies and areas where there was vegetation, and high temperatures (red hues) corresponded to exposed soils, increasing the rate of water evaporation. The images from 2015 and those from November and December 2019 presented the highest surface temperatures (greater than 45°C).

Figure 6. Surface temperature (°C). 11/21/2015 (A); 12/07/2015 (B); 07/18/2016 (C); 09/20/2016 (D); 06/22/2018 (E); 10/28/2018 (F); 11/13/2018 (G); 09/13/2019 (H); 10/15/2019 (I); 11/16/2019 (J); 02/12/2019 (K); and 12/20/2020 (L).

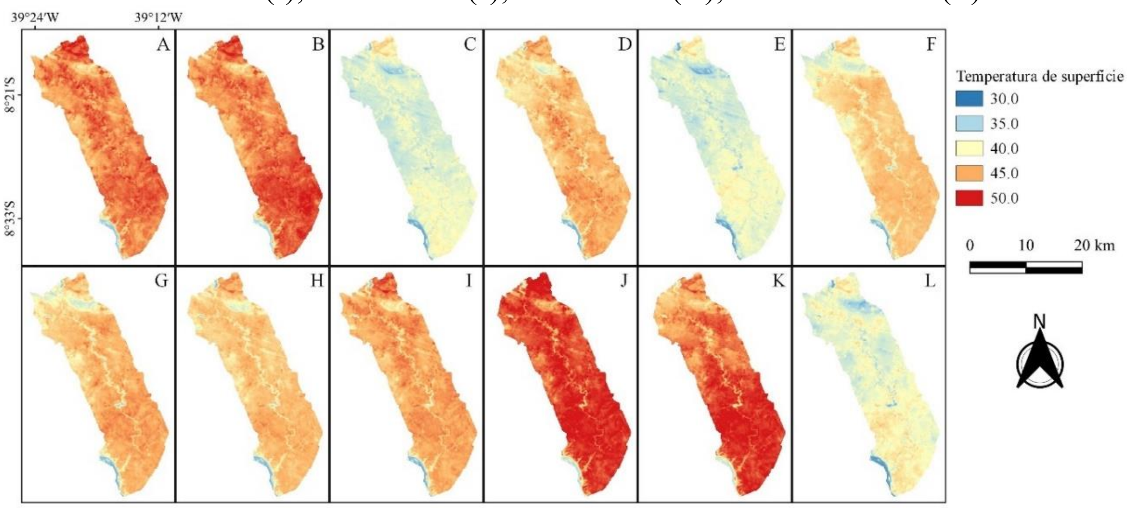

Figure 7 shows the spatial distribution of actual evapotranspiration (ETr) for each image. With respect to the NDVI, albedo, and surface temperature, only Figures 7C, 7E, and 7 L show greater spatial and temporal variations. According to Lins *et al*. (2017), actual daily evapotranspiration is directly related to the ability of vegetation to absorb moisture from the soil through its roots and transfer it to the atmosphere. Notably, water bodies are not represented in the images, as the SAFER model does not work for water bodies.

Figure 7. Actual evapotranspiration processed via the simple algorithm for evapotranspiration retrieval (SFAER). 11/21/2015 (A); 12/07/2015 (B); 07/18/2016 (C); 09/20/2016 (D); 06/22/2018 (E); 10/28/2018 (F); 11/13/2018 (G); 09/13/2019 (H); 10/15/2019 (I); 11/16/2019 (J); 02/12/2019 (K); and 12/20/2020 (L).

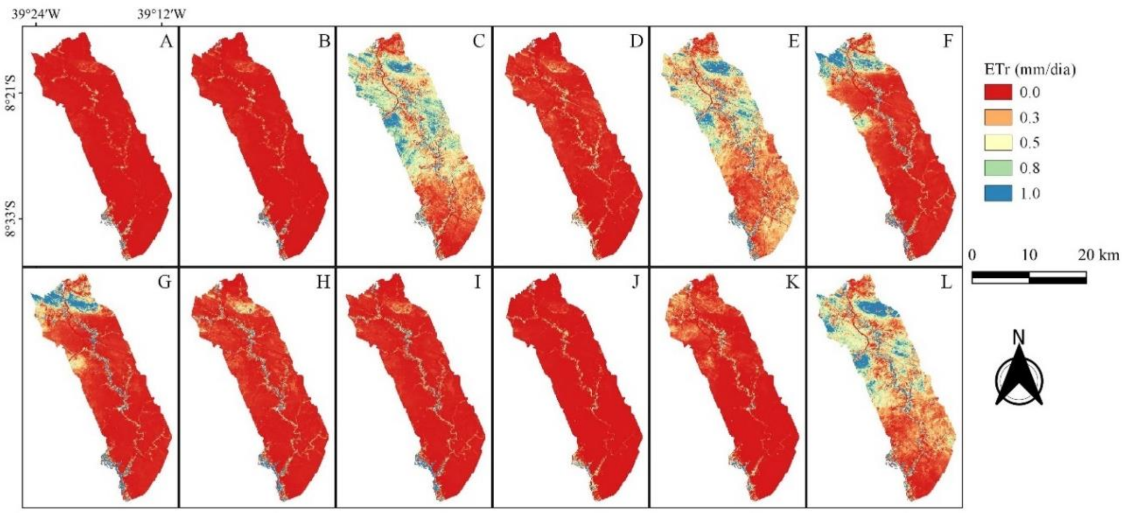

The regions with higher values of real evapotranspiration are linked to those with lower temperatures (Figure 6), with the opposite being true, since the more intense the evapotranspiration phenomenon is, the greater the transfer of latent heat and, therefore, the cooling of the surface; similar results were reported by Filgueiras *et al.* (2019) used SAFER to estimate $_{ETr}$ in São Desidério, BA.

Table 3 presents the descriptive statistics of actual evapotranspiration (ET_r) for the perennial stretch on the analyzed dates, with minimum, maximum, mean, standard deviation (SD), and coefficient of variation (CV) values, in addition to the reference evapotranspiration (ET_0) calculated via the Penman–Monteith method, which is based on climatological data from the automatic station Cabrobó, PE. The highest average values occurred on July 18, 2016, June 22, 2018, and December 20, 2020, all with ET $_{values}$ of approximately 0.4 mm/day. The coefficients of variation were generally high, confirming the high heterogeneity in land use and the dependence on the rainfall regime for the region's economic development. The maximum ET occurred on 12/07/2015, at 4.53 mm/day; on this date, the highest ET of 6.53 mm/day also occurred, as did the highest coefficient of variation (510.6%), as evidenced by the low average ET of 0.04 mm/day.

Table 3. Descriptive statistics of real evapotranspiration processed *via the simple algorithm for evapotranspiration retrieval* (SAFER).

Dates	ET_0 (mm/day)	Minimum	Maximum	Average	DP	CV (%)
		Actual evapotranspiration (mm/day)				
11/21/15	5.15	0.00	3.72	0.03	0.15	498.4%
12/07/15	6.53	0.00	4.53	0.04	0.19	510.6%
07/18/16	2.72	0.00	2.28	0.43	0.33	76.4%
09/20/16	2.49	0.00	1.82	0.05	0.11	230.2%
06/22/18	3.38	0.00	3.01	0.39	0.35	90.4%
10/28/18	4.18	0.00	3.02	0.18	0.33	185.0%
11/13/18	5.00	0.00	3.87	0.18	0.38	217.9%
09/13/19	4.82	0.00	3.51	0.10	0.26	264.9%
10/15/19	5.56	0.00	3.96	0.08	0.26	345.5%
11/16/19	2.81	0.00	1.84	0.02	0.11	427.2%
12/02/19	3.22	0.00	2.11	0.06	0.15	255.6%
12/20/20	3.57	0.00	3.15	0.40	0.38	95.5%

ET_0 = potential evapotranspiration; SD = standard deviation; and CV = coefficient of variation.

Using the SUREAL model, vegetation was classified along a 1.5-km stretch of each bank, as shown in Figure 8, distinguishing between cultivated areas (irrigated crops) and Caatinga areas (natural vegetation). The 2015 images (the period before the perennialization process produced by the PISF) show fewer irrigated areas along the Terra Nova River. Other images, after the stream's perennialization, show an increase in irrigated areas along the banks throughout the Terra Nova River. This indicates that the perennialization of streams, due to the release of water from the Terra Nova Reservoir, has enabled the growth of irrigated agriculture in the region by increasing water availability. However, this availability is still limited to areas close to banks. For areas further from banks, cropland is still highly dependent on rainfall.

Furthermore, from 2012--2016, one of the most severe droughts occurred, affecting the entire northeastern region of Brazil (CUNHA *et al*., 2018), which may explain the few cultivated areas (irrigated crops) in Figures 8A, 8B and 8D (from 2015--2016).

Figure 8. Classification of natural vegetation and cultivated areas processed by *the surface resistance algorithm* (SUREAL). 11/21/2015 (A); 12/07/2015 (B); 07/18/2016 (C); 09/20/2016 (D); 06/22/2018 (E); 10/28/2018 (F); 11/13/2018 (G); 09/13/2019 (H); 10/15/2019 (I); 11/16/2019 (J); 02/12/2019 (K); and 12/20/2020 (L).

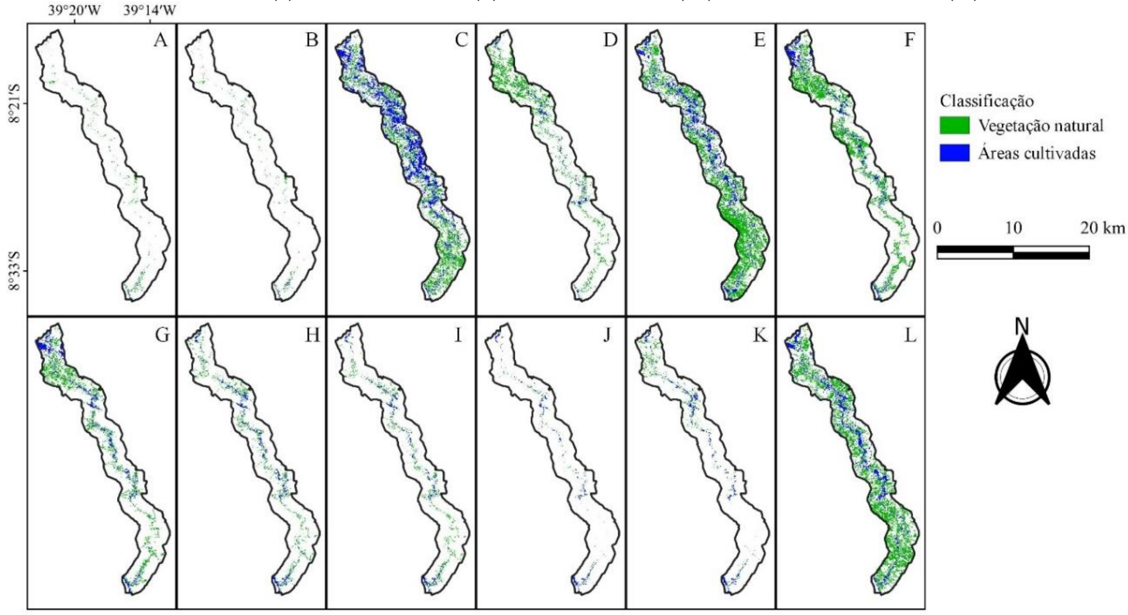

The total area of the SUREAL classification for natural vegetation and crops (irrigated crops) was defined, as shown in Figure 9. The increase in irrigated crops stood out on 06/22/2018 (15.2 km²) and 12/20/2020 (12.9 km²), conditioned by the greater rainfall in the region and on 07/18/2016, 10/28/2018 and 11/13/2018 (29.5, 7.7, and 7.6 km², respectively), possibly also due to the release of water from the PISF. The date of 09/13/2019 presented high previous precipitation of 90 days (59.6 mm); however, this precipitation was not accompanied by an increase in the areas of natural vegetation or irrigated areas.

Figure 9. Total area of natural vegetation classification and cultivated areas processed by *the surface resistance algorithm* (SUREAL) and accumulated antecedent precipitation values.

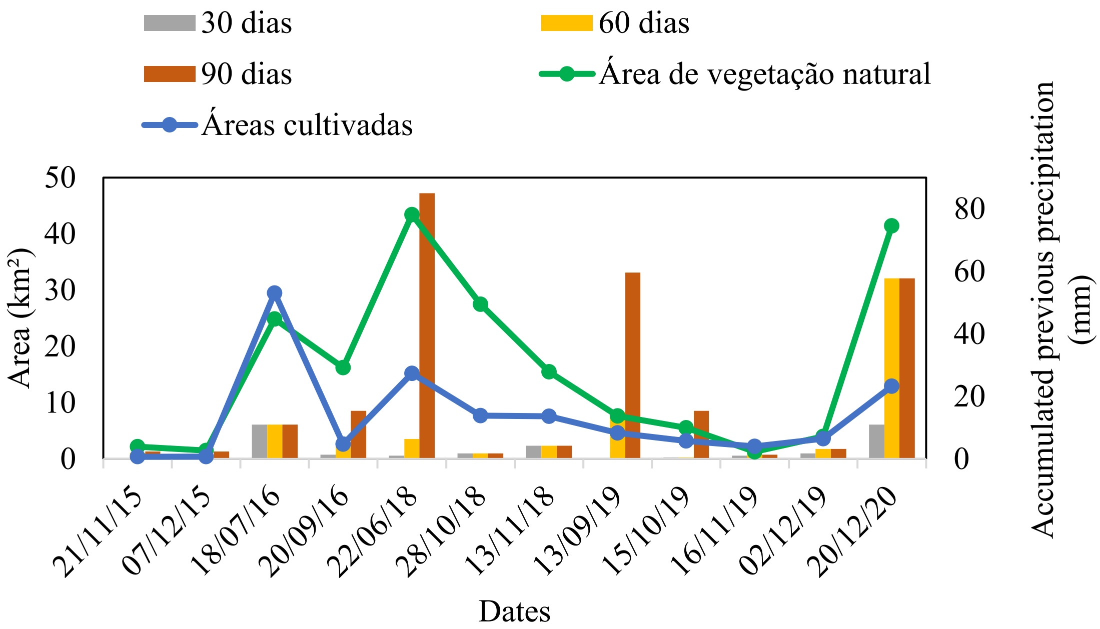

Therefore, precipitation remains highly relevant for the development of agricultural crops, especially in areas far from the banks of the perennial stretch of the Terra Nova Stream. According to Cunha *et al*. (2018) and Marengo, Torres, and Alves (2016), a greater frequency of severe droughts will likely increase the vulnerability of the Northeast Region of Brazil to drought in the near future. These projections suggest more frequent and intense droughts, as well as a trend toward desertification in the region. These conditions lead to increased evaporation from reservoirs and rivers, affecting irrigation and agriculture. This demonstrates the growing need to mitigate the effects of drought and develop coexistence with semiarid regions, such as the São Francisco River Integration Project (PISF), which aims to guarantee a water supply for the socioeconomic development of the states of northeastern Brazil that are most vulnerable to drought (IPEA, 2011).

The processing performed in this study was repeated 12 times (for each image) and took an average of a few seconds, considering all the source code developed, from the image definition (by ID, Table 1), calculation of planetary and surface albedo, NDVI, radiances of bands 10 and 11, brightness temperature and surface temperature (in K and °C), actual evapotranspiration (manually including the $ET_{0\ data}$ from the climatological station on the day of the image), to the completion of the image classification by SUREAL. Significant time savings were observed, as it was not necessary to download the raw images and perform the processing of the SAFER and SUREAL steps in conventional geoprocessing *software*, which can require many hours of processing.

6 CONCLUSIONS

Overall, there was an expansion of cultivated areas on the banks of the Terra Nova River, in the semiarid region of Pernambuco, between the Terra Nova Reservoir and the mouth of the Terra Nova

River, in the São Francisco River, and in the images from July 18, 2016, June 22, 2018, October 28, 2018, November 13, 2018, and December 20, 2020 (29.5; 15.2; 7.7; 7.6; and 12.9 km², respectively). In addition to the intensity of precipitation, the release of water from the São Francisco River Integration Project may have contributed to the increase in irrigated areas in the region.

The occurrence of rainfall is highly relevant for the development of agricultural crops, especially in areas far from the banks of perennial stretches.

Determining actual evapotranspiration and classifying vegetation via remote sensing techniques and implementing the SAFER and SUREAL models in a GHG environment are fast and effective tools. The models tested in this study are highly relevant for supporting environmental monitoring and planning, as well as water resource management in the region, across different sectors of society.

7 ACKNOWLEDGMENTS

The authors thank the Pernambuco State Science and Technology Support Foundation (FACEPE) for the funded project APQ 0300-5.03/17 and for the first author's postgraduate scholarship (IBPG-0855-5.03/20) and the Coordination for the Improvement of Higher Education Personnel (CAPES) for the financial support for the research.

8 REFERENCES

ALLEN, RG; PEREIRA, LS; RAES, D.; SMITH, M. **Crop Evapotranspiration** -Guidelines for computing crop water requirements. Rome: FAO, 1998. 297 p. (FAO Irrigation and Drainage paper 56) .

ALVARES, CA; STAPE, JL; SENTELHAS, PC; GONÇALVES, JLM; SPAROVEK, G. Köppen's climate classification map for Brazil. **Meteorologische Zeitschrift** , Berlin, vol. 22, no. 6, p. 711-728, 2013.

PERNAMBUCO WATER AND CLIMATE AGENCY. **Terra Nova Basin** . Recife: APAC, 2020. Available at: http://200.238.107.184/bacias-hidrograficas/40-bacias-hidrograficas/207-bacia-do-rio-terra-nova. Accessed on: May 6, 2021.

BECK, HE; ZIMMERMANN, NE; MCVICAR, TR; VERGOPOLAN, N.; BERG, A.; WOOD, EF Present and future Köppen-Geiger climate classification maps at 1-km resolution. **Scientific Data** , London, v. 5, no. 1, p. 1-12, 2018.

BEZERRA, BG; SILVA, BB; BEZERRA, JRC; BRANDÃO, ZN Real evapotranspiration obtained through the relationship between the FAO-56 dual crop coefficient and the NDVI. **Brazilian Journal of Meteorology** , São José dos Campos, v. 25, n. 3, p. 404-414, 2010.

CANCELA, JJ; GONZÁLEZ, XP; VILANOVA, M.; MIRÁS-AVALOS, JM Water Management Using Drones and Satellites in Agriculture . **Water** , Basel, vol. 11, no. 5, p. 874-878, 2019.

CHANDER, G.; MARKHAM, B.L.; HELDER, DL Summary of current radiometric calibration coefficients for Landsat MSS, TM, ETM+, and EO-1 ALI sensors. **Remote Sensing of Environment** , New York, vol. 113, no. 5, p. 893-903, 2009.

COLLISCHONN, B.; TUCCI, CEM Regional relationships between monthly precipitation and evapotranspiration. **Brazilian Journal of Water Resources** , Porto Alegre, v. 19, n. 3, p. 205-214, 2014.

MINERAL RESOURCES RESEARCH COMPANY. **Groundwater supply source registration project – Pernambuco** : Diagnosis of the municipality of Cabrobó. Recife: CPRM, 2005.

CUNHA, APMA; TOMASELLA, J.; RIBEIRO-NETO, GG; BROWN, M.; GARCIA, SR; BRITO, SB; CARVALHO, MA Changes in the spatial-temporal patterns of droughts in the Brazilian Northeast. **Atmospheric Science Letters** , Malden, vol. 19, no. 10, p. 1-8, 2018.

FILGUEIRAS, R.; MANTOVANI, EC; ALTHOFF, D.; DIAS, SHB; CUNHA, FF Sensitivity of evapotranspiration estimated by orbital images under the influence of surface temperature. **Agricultural Engineering** , Jaboticabal, v. 39, n. 1, p. 23-32, 2019.

GOOGLE EARTH ENGINE. **Google Earth Engine** . [*S. l.*]: Google, 2021. Available at: https://earthengine.google.com/. Accessed on: May 10, 2021.

GORELICK, N.; HANCHER, M.; DIXON, M.; ILYUSHCHENKO, S.; THAU, D.; MOORE, R. Google Earth Engine: planetary-scale geospatial analysis for everyone. **Remote Sensing of Environment** , New York , v. 202, no. 1, p. 18-27, 2017.

IBGE. **Panorama Cabrobó** . Brasília, DF: IBGE, 2021. Available at: https://cidades.ibge.gov.br/brasil/pe/cabrobo/panorama. Accessed on: May 10, 2021.

INCRA. **Land Market Analysis Report for the State of Pernambuco** (Jurisdiction of SR-03) - Partial . Recife: INCRA, 2016.

IPEA. **Transposition of the São Francisco River** : project opportunity analysis . Rio de Janeiro: IPEA, 2011.

LINS, FAC; ARAÚJO, DCS; SILVA, JLB; LOPES, PMO; OLIVEIRA, JDA; SILVA, ATGCSG Estimation of biophysical parameters and actual evapotranspiration in the semiarid region of Pernambuco using remote sensing. **Irriga** , Botucatu, v. 1, n. 1, p. 64-75, 2017.

MAPBIOMAS. **The project** . [*S. l.*]: MapBiomas , 2021. Available at: https://mapbiomas.org/o-projeto. Accessed on: October 5, 2021.

MARENGO, JA; ALVES, LM; BESERRA, EA; LACERDA, FF 2011. Climate variability and change in the Brazilian semiarid region. Water resources in arid and semiarid regions. **National Institute of Semiarid Region** , Campina Grande, p. 384-422, 2011.

MARENGO, JA; TORRES, RR; ALVES, LM Drought in Northeast Brazil - past, present, and future. **Theoretical And Applied Climatology** , Wien, vol. 129, no. 3-4, p. 1189-1200, 2016.

MONTENEGRO, AAA; ABRANTES, JRCB; LIMA, JLMP; SINGH, VP; SANTOS, TEM Impact of mulching on soil and water dynamics under intermittent simulated rainfall. **Catena** , Amsterdam, vol. 109, no. 1, p. 139-149, 2013.

OLIVEIRA, JDA; MOURA, GBA; NASCIMENTO, CR; LOPES, PMO; NÓBREGA, RS Assessment of Degradation and Environmental Changes in the Alto Ipanema Watershed. **Journal Brazilian Meteorology Institute** , São José dos Campos, v. 35, no. 4, p. 585-596, 2020.

ROUSE, JW; HAAS, RH; SCHELL, JA; DEERING, DW; HARLAN, JC **Monitoring the vernal advancement of retrogradation of natural vegetation** . Greenbelt : National Aerospace Spatial Administration , 1973.

SILVA, COF Supervised classification of irrigated area using spectral indices of Landsat-8 images with Google Earth Engine . **Irriga** , Botucatu , v. 25, n. 1, p. 160-169, 2020.

SILVA, COF; MANZIONE, RL; ALBUQUERQUE FILHO, J. Large-Scale Spatial Modeling of Crop Coefficient and Biomass Production in Agroecosystems in Southeast Brazil. **Horticulturae** , Basel, v. 4, no. 4, p. 44-64, 2018.

TEIXEIRA, AHC Determination of surface resistance to evapotranspiration by remote sensing parameters in the semiarid region of Brazil for land-use change analyses. *In* : NEALE, CMU; COSH, MH (org.). **Remote Sensing and Hydrology** . Jackson Hole : IAHS Press, 2012. v. 352, p. 167-170.

TEIXEIRA, AHC Determining Regional Actual Evapotranspiration of Irrigated Crops and Natural Vegetation in the São Francisco River Basin (Brazil) Using Remote Sensing and Penman–Monteith Equation. **Remote Sensing** , Basel, v. 2, no. 5, p. 1287-1319, 2010.

TEIXEIRA, AHC; BASTIAANSSEN, WGM; AHMAD, MD; BOS, MG Reviewing SEBAL input parameters for assessing evapotranspiration and water productivity for the Low-Middle São Francisco River basin, Brazil. **Agricultural and Forest Meteorology** , Amsterdam, v. 149, n. 3-4, p. 462-476, 2009.

TEIXEIRA, AHC; HERNANDEZ, FBT; LOPES, HL; SCHERER-WARREN, M.; BASSOI, LH **Spatiotemporal modeling of energy and water balance components in the Brazilian Semiarid Region** . Campinas: Embrapa Semiárido, 2013.

TEIXEIRA, AHC; LEIVAS, JF; HERNANDEZ, FBT; FRANCO, RAM Large-scale radiation and energy balances with Landsat 8 images and agrometeorological data in the Brazilian semiarid region. **Journal of Applied Remote Sensing** , Bellingham, vol. 11, no. 1, p. 16-30, 2017.

TEIXEIRA, AHC; PADOVANI, C.; ANDRADE, R.; LEIVAS, JF; VICTORIA, D.; GALDINO, S. Use of MODIS Images to Quantify the Radiation and Energy Balances in the Brazilian Pantanal. **Remote Sensing** , Basel, v. 7, no. 11, p. 14597-14619, 2015.

TEIXEIRA, AH C; LEIVAS, JF; STRUIVING, T.; REIS, J.; SIMÃO, F. Energy balance and irrigation performance assessments in lemon orchards by applying the SAFER algorithm to Landsat 8 images. **Agricultural Water Management** , Amsterdam, v. 247, p. 106725, 2021.

TEIXEIRA, AHDC; HERNANDEZ, FBT; ANDRADE, RG; LEIVAS, JF; BOLFE, EL Energy balance with Landsat images in irrigated central pivots with corn crop in the São Paulo State, Brazil. **SPIE** , [*S.l.*] , v. 1, no. 16, p. 1-10, 2014.

UNITED STATES GEOLOGICAL SURVEY. **EarthExplorer** . Washington, DC: USGS, 2021. Available in : https://earthexplorer.usgs.gov/. Access on : May 10, 2021.

UNITED STATES GEOLOGICAL SURVEY. **Landsat 8 (L8) Data Users Handbook** . Sioux Falls: USGS, 2016.

UNITED STATES GEOLOGICAL SURVEY (USGS). **Landsat 8 Collection 1 (C1), Land Surface Reflectance Code (LaSRC), Product Guide** . Dakota: USGS, 2020.

VENANCIO, LP; MANTOVANI, EC; AMARAL, CH; NEALE, CMU; FILGUEIRAS, R.; GONÇALVES, IZ; CUNHA, FF Evapotranspiration mapping of commercial corn fields in Brazil using SAFER algorithm. **Scientia Agricola** , Piracicaba, v. 78, n. 4, p. 1-12, 2021.